PAPER

Reversible addition–fragmentation chain transfer depolymerization of poly(methyl methacrylate) in toluene

Don X. Bones,[a] Adarsh Kumar,[b] Emily Nelson,[b] Bryanna Fofie,[b] Erik P. Hoy [ID] [b] and William M. Gramlich [ID] *[a,c]

Controlled depolymerizations of poly(methyl methacrylate) (PMMA) *via* reversible addition fragmentation chain transfer (RAFT) reach higher yields in some solvents rather than others, and the exact reasons are not fully understood. PMMA was synthesized with trithiocarbonate (TTC) and dithiobenzoate (DTB) end groups to study depolymerization in toluene, which has been reported to have a lower monomer yield than other solvents. In toluene, the depolymerization kinetics were found to have two regions: one assisted by solvent-derived impurities and another being primarily self-initiation. Using a rate order analysis, we found evidence that initiation can lead to simultaneous homolysis of the RAFT end group and the depropagation of one monomer. Additionally, DTB end groups had a greater tendency than TTC end groups to undergo elimination, terminating the active depropagating center and limiting depolymerization extent. Radical thermal initiators were added into PMMA depolymerizations in toluene, demonstrating that di-*tert*-butyl peroxide can increase the conversion of polymer to monomer for TTC end groups.

Introduction

Scientists continue to combat the ongoing crisis of plastic waste by developing new materials and techniques that will reduce pollution. A common technique is mechanical recycling, where mixed waste is physically separated, melted, and formed into flakes and pellets for future use.[1] Unfortunately, this technique cannot be applied to plastics that degrade significantly when reprocessed. In such cases, the heat-sensitive plastic must be recycled chemically. Chemical recycling converts solid plastic waste into valuable commodities, often in the form of monomers or fuels, recapturing much of the energy to produce the original molecules.[2]

Polymers with ester groups in their backbone (*e.g.*, poly(lactic acid) and poly(ethylene terephthalate)) are susceptible to chemical recycling techniques, due to their susceptibility towards solvolysis.[2] Conversely, vinyl polymers, with backbones that consist entirely of carbon–carbon bonds, often require high-temperature pyrolysis to decompose into smaller molecules, generating a mixture including monomers. Some

methacrylate polymers can primarily decompose into their respective monomer along with some impurities. For example, the pyrolysis of stabilized poly(methyl methacrylate) (PMMA) at 400 °C yields a mixture of methyl methacrylate (MMA), ethyl acrylate, and other chemicals due to degradation at these elevated temperatures.[3] The impure crude product must be purified, increasing the cost and decreasing the yield of the chemical recycling process. To avoid the challenges with purification, reactions must occur at temperatures high enough to facilitate depolymerization, but low enough to avoid the formation of impurities.

Controlled depolymerizations, defined as the reverse of controlled polymerizations that utilize the same methods to reduce irreversible termination,[4] can overcome these challenges by functionalizing a polymer with an end group[4] or comonomer[5] that, when activated by external stimuli, generates active centers. After initiation, the active center concentration is controlled by a reversible deactivation equilibrium to minimize termination while allowing depropagation to occur. For PMMA, two classes of controlled depolymerization have been studied: atom transfer radical polymerization (ATRP)[6,7] and reversible addition fragmentation chain transfer (RAFT) polymerization.
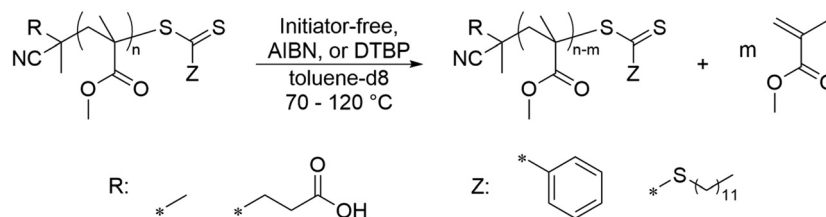
RAFT polymerizations of PMMA often generate a polymer with a trithiocarbonate (TTC) or dithiobenzoate (DTB) end group due to their controlled MMA RAFT polymerizations.[8] The controlled depolymerization of RAFT methacrylates in the

[a]Department of Chemistry, University of Maine 156 Aubert Hall, Orono, ME 04469, USA. E-mail: William.gramlich@maine.edu

[b]Department of Chemistry and Biochemistry, Rowan University, Glassboro, NJ 08028, USA

[c]Advanced Structures and Composites Center, University of Maine, Orono, ME 04469, USA

Scheme 1 Depolymerization of PMMA-RAFT with and without the radical initiators azobis(2-methylpropionitrile) (AIBN) and di-*tert*-butyl peroxide (DTBP).

absence of an initiator was first witnessed using oligo-dimethylsiloxane and oligo-ethylene glycol terminated with methyl methacrylate in dioxane at 70 °C with repeat unit concentrations of 0.1 M.[9] Both poly(methacrylates) depolymerized to approximately 30 mM monomer concentration and reached equilibrium in 48 hours. Size exclusion chromatography indicated controlled depolymerizations because the molecular weight decreased due to the chain transfer mechanisms allowing all polymers to depolymerize evenly. The radical inhibitor, butylated hydroxy toluene, inhibited depolymerization, suggesting that the depolymerization proceeded *via* a radical mechanism.

Since then, others have continued to explore and refine RAFT poly(methacrylate) depolymerizations. For example, the Anastasaki group conducted depolymerizations at 120 °C at 5 mM repeat unit concentration on various methacrylate repeat units, reaching >90% depolymerization of repeat units to monomer.[10] Later, this reaction was optimized using a flow reactor and in-line dialysis at 160 °C and 1 M repeat unit concentration, reaching 68% depolymerization.[11] Controlled depolymerizations of MMA have also been investigated with various end-groups and solvents. They found that dithiobenzoate terminated PMMA (PMMA-DTB) liberated more monomer than trithiocarbonate terminated PMMA (PMMA-TTC) and that depolymerizations should be performed in a dioxane solvent for greater yields under their conditions.[12] Furthermore, they functionalized the dithiobenzoate end group with electron donating groups and achieved depolymerization yields of 75% at 90 °C within 8 hours.[13] However, most research efforts did not explore the practicality of RAFT depolymerizations in chemical recycling, specifically whether the end groups are preserved at the end of the service life of the polymer. Despite the recent research in PMMA-RAFT depolymerizations, why some solvent and RAFT end group systems depolymerize better than others is unclear.

Furthermore, questions still exist regarding the exact mechanisms of initiating PMMA-RAFT depolymerizations without the addition of external initiators in different solvents. The Anastasaki group has investigated the fate of the RAFT end group for PMMA-RAFT depolymerizations using dioxane and p-xylene as solvents, and DTB and TTC as RAFT end groups.[14] Regardless of the conditions employed, unimers and solvent-derived RAFT products were observed. The solvent-derived RAFT products suggested that one of the potential initiation mechanisms originates from solvent-derived radicals. However, currently reported results have not confirmed the common hypothesis for PMMA-RAFT depolymerizations that it initiates *via* the thermal homolysis of the C–S linkage between the polymer and RAFT end group.

This current investigation aims to understand how solvents with lower monomer yields, like toluene, facilitate PMMA-RAFT depolymerizations by studying their kinetics to yield a mechanistic understanding and discover opportunities for improvement and optimization. To this end, we prepared PMMA-TTC and PMMA-DTB, dissolved them in toluene-d8, and depolymerized them under various end group concentrations, temperatures, and radical initiators (Scheme 1). With these variations, we monitored monomer evolution and end group degradation, discovering that PMMA-TTC depolymerized to a higher extent than PMMA-DTB in toluene which is different than depolymerizations in 1,4-dioxane. The kinetics data were then used to support hypothesized mechanisms and compare the two RAFT end groups in toluene. In doing so, we found that initiation by C–S homolysis of the end group fails to completely describe the system properly and that the RAFT end groups explored have similar degradation rates. The analysis of the mechanisms of RAFT depolymerizations and the different behavior between RAFT end groups in toluene provides valuable information to improve and optimize depolymerizations for chemical recycling.

Materials and methods

Anhydrous 1,4-dioxane (Sigma-Aldrich), toluene-d8 (Thermoscientific), and di-*tert*-butyl peroxide (DTBP) (TCI) were used as received. Stabilized methyl methacrylate (Thermoscientific) was purified by passing through a basic alumina column. 2,2′-Azobis(2-methylpropionitrile) (Sigma-Aldrich) was purified by recrystallization in methanol. Chain transfer agents (CTA) 4-cyano-4-(dodecylsulfanylthiocarbonyl) sulfanyl pentanoic acid[15] (TTC) and 2-cyano-2-propyl benzodithioate[16] (DTB) were synthesized according to literature.

RAFT polymerization of poly(methyl methacrylate)

RAFT polymerizations were performed with a molar ratio of [MMA] : [CTA] : [AIBN] = 50 : 1 : 0.2 in anhydrous 1,4-dioxane with an MMA concentration of 0.2 g mL^{-1}. The reaction

mixture was degassed by three freeze–pump–thaw cycles, and then heated at 70 °C for 7 hours (TTC) or 8 hours (DTB), to achieve approximately 80% monomer conversion. The polymerization was then quenched by cooling in a water ice bath. After quenching, the volatiles were removed *in vacuo*, and the crude PMMA-TTC and PMMA-DTB were precipitated in 10-fold excess methanol 3 times. The purified product was then analyzed by ^{1}H NMR spectroscopy and size exclusion chromatography (SEC). ^{1}H NMR spectroscopy was used to determine the number of average molecular weights of the polymer through end group analysis (Fig. S5 and S6). SEC indicated a low relative dispersity to confirm a successful controlled RAFT polymerization (Fig. S7 and S8).

Monomer equilibrium determination

Additional polymerizations were performed at 90 °C and 120 °C to approximate the monomer equilibrium concentration (Table S1). All polymerizations were degassed by three freeze–pump–thaw cycles in a Schlenk flask. Polymerizations were first performed at monomer concentrations of 200 mM at 120 °C and 100 mM at 90 °C for 24 hours with molar ratios [MMA] : [TTC] : [I] = 36 : 1 : 0.2, where [I] is AIBN for 90 °C and DTBP for 120 °C. The solutions were then cooled in ice and removed of volatiles. The number average molecular weight of the polymer was determined by ^{1}H NMR spectroscopy using end group analysis to determine the final monomer concentration in the reaction mixture after quenching. Additional polymerizations were performed to determine if the final monomer concentration was a result of exhausting initiating species or an equilibrium between propagation and depropagation. In general, subsequent polymerizations were performed with a monomer concentration 10–15 mM higher than the previous final monomer concentration. This process was repeated until a polymerization yielded a monomer concentration that was equivalent to the previous trial or equivalent to the greatest monomer concentration yielded from any depolymerization (Table S1).

Controlled depolymerization of PMMA-CTA

Solutions of PMMA-RAFT in toluene-d8 were prepared in 5 mm diameter, precision Wilmad® NMR tubes. For depolymerizations with initiators, the AIBN or DTBP were dissolved in toluene-d8 and included. The NMR tube was then degassed by three freeze–pump–thaw cycles and flame sealed under reduced pressure. An ^{1}H NMR spectrum was collected to determine the initial monomer concentration. The NMR tube was then heated in an oil bath for a predetermined time and temperature to facilitate depolymerization. For each time point, depolymerization was then quenched by immersing the NMR tube in ice, an NMR spectrum was collected, and then heated once again. This heat–quench–cool cycle was repeated until all desired NMR spectra were acquired. A selection of the depolymerization trials was then analyzed by SEC. The heat–quench–cool cycles were not performed for experiments that required less than 15 minutes of heating per cycle. Rather, a single sample in an NMR tube was heated for a predetermined time for each point in the depolymerization curve.

^{1}H NMR spectroscopy

Purified polymers and RAFT agents were dissolved in 0.6 mL of deuterated chloroform (CDCl$_3$) and analyzed on a Bruker Ascend 500 MHz NMR spectrometer. Data was obtained and processed with MestReNova14 ^{1}H NMR software. Spectra were referenced to residual CHCl$_3$ (7.265 ppm). All depolymerizations were performed in toluene-d8 which was referenced to residual toluene methyl protons (2.08 ppm).

Quantification of PMMA end groups and monomers was achieved by using the methyl ester protons of MMA monomer and repeat units (3.23–3.65 ppm)[17] as internal standards. This assumed that no monomers escaped the flame sealed NMR tube or degraded. Monomer concentration was determined by using a vinyl peak at 6.03 ppm.[9] The TTC end group concentration was determined by using the methylene proton adjacent to the thiol of the dodecyl group peak at 3.03 ppm.[15] The DTB end group concentration was determined by using the phenyl group meta protons peak at 7.90 ppm.[16] Unsaturated end group concentration was determined by using a vinyl peak at 6.14 ppm.[17]

Size exclusion chromatography

Size exclusion chromatography was performed with a 5 mg mL^{-1} concentration of polymer in solvent. Solutions were passed through a 0.2 μm PTFE syringe filter prior to injection on an Agilent 1260 Infinity Size Exclusion Chromatograph equipped with a temperature-controlled refractive index detector. For all samples, HPLC grade THF was used as the eluent at a 1 mL min^{-1} flow rate and operating temperature of 35 °C. The SEC was equipped with three Phenogel columns with different pore sizes (Phenomenex Organic columns, 50 Å, 10^3 Å, and 10^6 Å) and calibrated with polystyrene standards.

Inductively coupled plasma mass spectrometry

The impurities of toluene-d8 were collected by evaporating 3 mL of toluene-d8 and 1 mL Milli-Q water in glass vials followed by rinsing the vials with 3 mL Milli-Q water. Samples were then acidified using Optima double distilled nitric acid to 1% acid. Samples were run using a Thermo Element 2 inductively coupled plasma-sector field mass spectrometer (ICP-MS). The sample introduction system consisted of an Elemental Scientific (ESI) DX-4 autosampler with a PFA nebulizer self-aspirated at 100 μL min^{-1}. The instrument was tuned each day to optimize the signal and minimize oxides. The samples were analyzed for ^{56}Fe, ^{60}Ni, ^{63}Cu, and ^{32}S, all measured in medium resolution. The instrument was calibrated before each run and a reference sample, SLRS-6 from National Research Council Canada, was run as a quality control sample.

Computational methods

All the structures of the polymer chains used in the simulation were fully optimized at the M06-2X/def2TZVP level of

theory[18,19] without any constraints using the Gaussian 16 program.[20] Each polymeric system was modeled as two monomeric chain units attached to the RAFT end groups TTC, DTB, *O*-ethyl dithiocarbonate (DTO), 1-pyrrolecarbodithioate (DTP), and *N*-pyridine carbonodithiaote (PCDT). To identify the best possible depolymerization pathway, the structures were optimized first to potential global minimum (GM) structures by performing a conformational search and explicitly sampled low-lying local minima in the predicted GM neighborhood. A systematic conformational search on TTC and DTB were performed using the ABCluster Program.[21,22] These conformational searches were carried out at the GFN2-xTB level of theory with thorough and explicit dihedral sampling, resulting in the generation of 1500 different conformers for each TTC and DTB. Transition-state searches were initiated from each refined conformer to capture possible kinetic advantages arising from conformational diversity. While the predicted global-minimum (GM) conformer is the thermodynamically most stable, a local-minimum conformer 4.07 kcal mol^{-1} above the GM for TTC and 6.77 kcal mol^{-1} above the GM for DTB delivered a lower activation barrier. Accordingly, the lowest $\Delta G^{\ddagger}$ (kinetically controlled barrier) is presented in support of our experimental results, while the GM-based analysis wherein the six lowest-energy conformers for both TTC and DTB were subsequently optimized at the M06-2X/def2-TZVP level of theory without constraints using the Gaussian 16 program is provided in the Supplementary Information (SI).

The free energy landscapes for the decomposition reactions were explored using the DFT-based metadynamics. To attain the desired reactions, the breaking of bonds in the depolymerization reactions was biased using three collective variables (CVs): the distances between Carbon–Sulfur (CV$_1$), Carbon–Carbon (CV$_2$), and Carbon–Hydrogen (CV$_3$). The bond distances were monitored and confined with quadratic walls at 8.0 Å and a force constant of 100.0 kcal mol^{-1} Å^{-2}. The dimensions of the model system in the non-periodic box defined to perform the metadynamics were 30 × 30 × 30 Å^3. The Gaussian bias potential, characterized by a height of 0.25 kcal mol^{-1} and a width of 0.15, was introduced at intervals of every 25-time step throughout the simulation. The simulations were performed using the CP2K program.[23,24] A double zeta valence polarized basis set, optimized for the Goedecker, Teter, and Hutter (GTH) pseudopotential[25–27] was employed in the calculations. These simulations used the PBE functional[28] in conjunction with Grimme's DFT-D3 dispersion correction, which was applied with zero damping.[29] The NVT ensemble was utilized, and temperature control at 393.15 K was achieved using a thermostat based on canonical sampling through velocity rescaling (CSVR).[30] Further, a cutoff parameter of 360 Ry and a relative cutoff of 60 Ry were used for the basis set defined for the simulation. The graph.psmp program incorporated in the CP2k software package[23] was employed to explore the free energy surface (FES)[31–33] and minimum energy path.

Results and discussion

Initial rates of depolymerization

Previous reports have demonstrated that in a solution of dioxane PMMA-DTB depolymerizes faster and with a greater yield than PMMA-TTC.[12,34] However, in toluene, which has not been reported as a solvent for PMMA-TTC depolymerization, PMMA-TTC depolymerized faster and to higher monomer concentrations than PMMA-DTB regardless of the end group concentration and temperature used (Fig. 1a and b). This faster and higher yield with PMMA-TTC in toluene *versus* PMMA-DTB in dioxane suggests that the solvent type can affect the effectiveness of a particular end group for depolymerization. An equilibrium kinetics model was used to linearize the depolymerization progress curves in Fig. 1a and b (eqn (1), see SI for derivation):

$$\ln\left(\frac{[\mathrm{M}]_{\mathrm{eq}} - [\mathrm{M}]_0}{[\mathrm{M}]_{\mathrm{eq}} - [\mathrm{M}]_t}\right) = k_{\mathrm{p}}[\mathrm{P}^{\bullet}]t \tag{1}$$

where k_{p} is the rate constant for propagation, $[\mathrm{P}^{\bullet}]$ is the active center concentration, $[\mathrm{M}]_{\mathrm{eq}}$ is the equilibrium monomer concentration, $[\mathrm{M}]_t$ is monomer concentration at time t, and $[\mathrm{M}]_0$ is the initial monomer concentration. Eqn (1) indicates that a linearized depolymerization curve with a constant $[\mathrm{P}^{\bullet}]$ will yield a straight line. Linearized depolymerization curves at 90 °C matched the model well, as a clear linear slope was observed with a y-intercept near 0 mM, indicating that controlled depolymerization followed the equilibrium model (Fig. 1c). However, linearized depolymerization kinetics at 120 °C were only linear after 15 minutes and failed to intersect with the origin (Fig. 1d), suggesting a difference in active center concentration before and after 15 minutes. After 15 minutes, the depolymerizations at 120 °C appeared to follow controlled depolymerization.

The apparent activation energy of these depolymerizations can be used to compare the lability of the end groups to different linkages within PMMA. PMMA-TTC and PMMA-DTB had apparent activation energies of 13 ± 3 and 24 ± 3 kcal mol^{-1}, respectively, which is significantly lower than potential other linkages in PMMA (see SI). Computational analysis of the depolymerization mechanism in the gas phase yielded activation energies of 17 and 25 kcal mol^{-1} for PMMA-DTB and PMMA-TTC, respectively (see SI for more details). This relative agreement between experimental and gas phase computations suggests that the apparent activation energies experimentally observed in toluene are due to the fragmentation of the RAFT end group initiating the depolymerization and not due to toluene. These results are consistent with literature reported bulk depolymerizations where PMMA-TTC depolymerized at lower temperatures than PMMA-DTB which was attributed to a stronger C–S bond for PMMA-DTB than PMMA-TTC.[35,36] Since solvent-free gas phase computations and bulk depolymerizations have similar reactivities to depolymerizations in toluene, toluene does not appear to significantly affect the initiation step of polymerization. Since this behavior is the opposite of
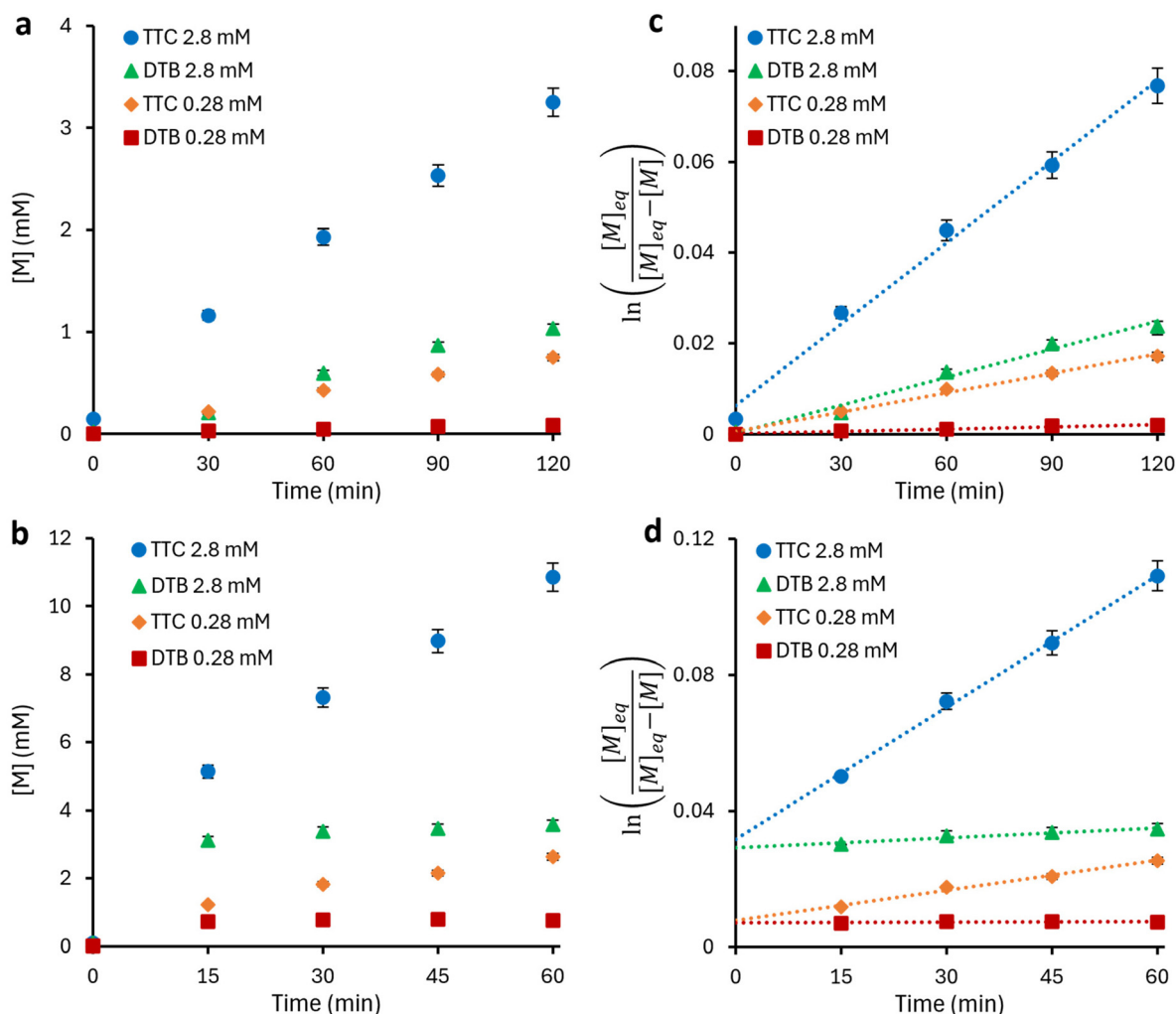
Fig. 1 The concentration of monomer in solution, [M], for depolymerizations of PMMA-TTC and PMMA-DTB at end group concentrations of 0.28 mM and 2.8 mM, or repeat unit concentrations of 10 mM and 100 mM respectively, at (a) 90 °C and (b) 120 °C. Depolymerization curves linearized using eqn (1), with $[M]_0$ equal to zero, for (c) 90 °C and (d) 120 °C. Error bars are one standard error with n = 2 replications. The linear fits of graph d are extrapolated to the ordinate.

1,4-dioxane, the results suggest that 1,4-dioxane does affect the reactivity of the end group.

The relative reactivity of the two RAFT end groups is different than that previously reported in different solvents. The Anastasaki group[12] found that PMMA-DTB depolymerized faster than PMMA-TTC at 67 μM end group concentration in 1,4-dioxane at 120 °C. In their work, they attributed the difference in depolymerization rates to the difference in the strength of the C–S bond between the RAFT end group and the polymer. However, if this difference in depolymerization rates was only due to the C–S bond strength, we would expect the same relative rates regardless of the reaction concentration and solvent at 120 °C. Additionally, deviations in PMMA-DTB rate trends could also be due to a competing reaction where elimination by the Chugaev elimination is preferred over homolysis of the C–S bond.[37] Furthermore, solvent molecules can stabilize transition states, allowing C–S bonds to break

more easily in different solvents, potentially explaining the different behavior in 1,4-dioxane.[38] Finally, 1,4-dioxane has been shown to react with RAFT end group fragments during depolymerization, which could also explain the relative reactivity discrepancy between depolymerizations in different solvents.[14]

Evidence of impurity assisted depolymerization

Depolymerizations at 120 °C failed to follow the equilibrium model early in the reaction because the fit (Fig. 1d) did not intersect at the origin. This behavior appears to be due to a greater active center concentration within the first 15 minutes. A separate study was performed within 15 minutes to analyze the depolymerization of PMMA-DTB at short intervals (Fig. 2a). The curve shows a sharp increase in monomer evolution and thus, depolymerization rate within the first 5 minutes. After 5 minutes, the rate of depolymerization drasti-
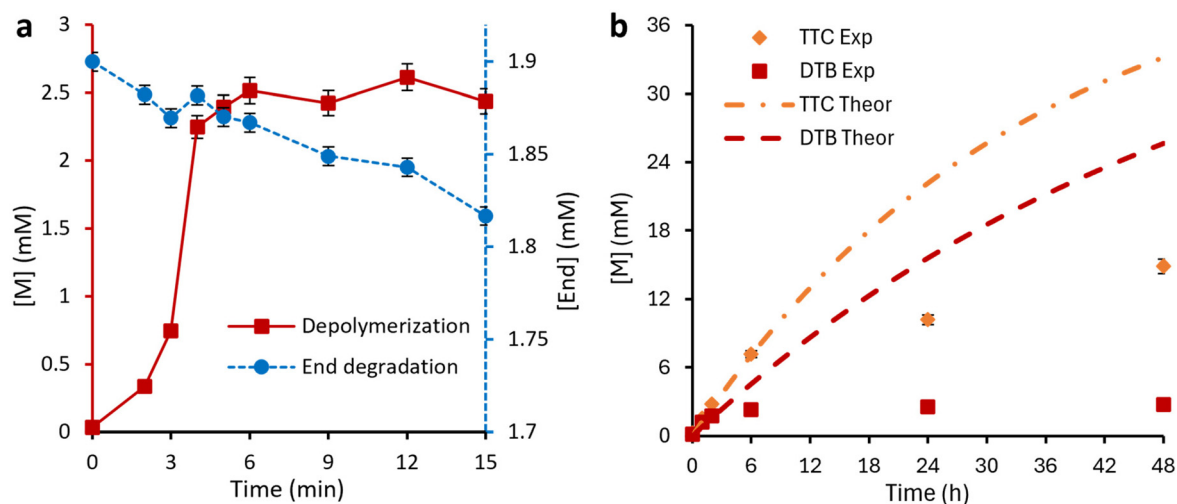
Fig. 2 (a) Depolymerization of PMMA-DTB at 120 °C and 1.9 mM end group concentration (left axis, solid red line, squares) and the concentration of remaining DTB end group (right axis, dashed blue line, circles) with respect to time. (b) Depolymerization of PMMA-DTB and PMMA-TTC at 90 °C for 48 hours with an end group concentration of 5.56 mM, or a repeat unit concentration of 200 mM (Exp). The expected result of the depolymerization curve using the initial rate and eqn (1) (Theor). Error bars are one standard error with n = 2 replications.

cally decreases, and monomer concentration nearly plateaus, yielding a discontinuous trend in monomer evolution. For depolymerizations at 90 °C, a discontinuity was not as visually clear (Fig. 2b). To determine whether these depolymerization curves exhibit any discontinuities and determine the origin of the discontinuity, further analysis was needed.

Literature has suggested that some initiation in a controlled RAFT depolymerization occurs at the RAFT end group *via* thermal homolysis of the C–S bond present at the terminal repeat unit.[10,34,36] Since this initiation mechanism creates a thiol-centered radical as well, it can result in some fraction of RAFT end groups degrading as a side reaction and consequently decrease the end group concentration. Thus, the trends in end group concentration should follow those in monomer concentration over time if the initially higher active center concentration is due to end groups undergoing homolysis. Depolymerization of PMMA-DTB (Fig. 2a) had a steady decrease of 4.9 ± 0.4 μM s^{-1} in end group concentration within a 15-minute depolymerization, indicating no change in the end group degradation rate, while having a significant change and discontinuity in monomer generation rate. Since no discontinuity exists for the degradation of the end group, the change in active center concentration, and thus change in the rate of monomer generation, observed is partially independent of the end group concentration. This behavior suggests that another species exists in the toluene that can generate radicals that can react with RAFT chain ends to form active centers. These impurities are consumed within 5 minutes at 120 °C, leading to a slower depolymerization rate.

The PMMA-DTB and PMMA-TTC linearized depolymerization curves in Fig. 1d are also consistent with initial rates of depolymerization being faster due to impurities assisting initiation. The linear fit of the 15–60 minutes region extrapolated to the ordinate yields monomer concentrations of 3.2 ±

0.2 and 0.78 ± 0.06 mM for end group concentrations of 2.8 and 0.28 mM, respectively. This monomer concentration appears to correlate to the monomers generated by impurities initially assisting the depolymerization. For PMMA-DTB and PMMA-TTC depolymerizations with identical end group concentrations, the monomer concentrations generated by impurities are nearly equivalent to one another, as suggested by the extrapolations' intersection near the ordinate. Interestingly, even though PMMA-TTC depolymerized faster than PMMA-DTB, the extrapolations' intersection at the ordinate suggests that the monomer generated by impurities is independent of the RAFT end group used.

For experiments at 90 °C, no noticeable discontinuities existed within the first two hours (Fig. 1a). However, around 2 and 6 hours the rate law appears to change for PMMA-DTB and PMMA-TTC, respectively (Fig. 2b). Eqn (1) was used to model the expected RAFT depolymerization by fitting the first 2 hours of the depolymerization curves in Fig. 2b and predicting theoretical future monomer concentrations, assuming a steady state active center concentration. This theoretical curve predicts a significantly higher concentration at 24 and 48 hours than observed. This suggested that the active center concentration does not remain constant throughout the 48-hour depolymerization. This behavior suggests that like at 120 °C, early in the depolymerization at 90 °C a greater active center concentration exists from radical generating impurities that initiate depolymerization. At 90 °C, the impurity assisted region lasts longer because the half-life of the radical generating impurities is significantly greater at reduced temperatures as expected by an Arrhenius relationship. Once the impurities are mostly consumed at around 2–6 h, the depolymerization likely is primarily initiated by RAFT end group homolysis.

The presence of initiating impurities in solvents is supported by Wang *et al.*'s investigation on the solvent effects of

RAFT depolymerizations.[12] Their analysis showed that the depolymerization conversions for xylene, toluene, and benzene were significantly different under the same conditions which was attributed to polarity differences.[38] However, the dielectric constants of xylenes, toluene, and benzene are 2.4, 2.38, and 2.28, respectively, which are not large differences.[39] Rather, the results of Wang *et al.* suggest that the different behavior for these three solvents could be due to varying concentrations of impurities that can initiate depolymerizations. This behavior would also explain why depolymerizations in 1,4-dioxane have faster rates than toluene, since 1,4-dioxane generates peroxides that can generate radicals.[12] Evidence of impurity assisted initiation was reported by Häfliger *et al.* who found solvent-derived moieties covalently bonded to the RAFT group for xylene,[14] which may have been due to trace metals, sulfur-containing compounds, or other impurities in toluene.

In our current study, we performed ICP-MS on toluene-d8 and found that iron, copper, and nickel were present at approximately 1 ppb, while sulfur atoms were present at 300 ppb. These metals have been shown to initiate RAFT polymerizations.[40] Additionally, some sulfur oxyanions are reducing agents that can initiate.[41] We performed a depolymerization of PMMA-DTB at 120 °C using distilled toluene-d8 (Fig. S9) to see if this would affect the concentration of monomer evolved due to impurities. The monomer concentration evolved *via* impurity assistance for non-distilled toluene-d8 was 4.2 mM (*n* = 3 replications, 95% CI [3.4, 5.0]). Using distilled toluene-d8, the monomer concentration evolved dropped to 3.7 mM, remaining within the 95% confidence interval of the non-distilled toluene-d8 trials. This suggests that the impurities assisting depolymerization were not the metals in the solvent found by ICP-MS. The impurities assisting the depolymerization may have been unsuccessfully removed by distillation or originated from contact with glassware and needles during solvent transfer to the reaction vessel. The impurities also may have originated from the purified polymer, such as trace AIBN that was not fully removed by precipitation after synthesis or trace metals, or from auto-oxidized toluene from trace oxygen remaining in the system.[42] Future more detailed studies are required to confirm the identity of these impurities.

End group order analysis

To understand the depolymerization initiation mechanism, the reactant order of the end group for depolymerization was determined with eqn (2) (see SI for derivation):

$$\ln R_d = \ln k_{app} + a(\ln[End]) \qquad (2)$$

where R_d is the initial rate of depolymerization, k_{app} is the apparent rate constant, [End] is the concentration of end groups, and a is the end group order with respect to the evolution of monomer. The initial rates were measured for PMMA-TTC and PMMA-DTB depolymerizations at 90 and 120 °C (see Fig. 1) and used to analyze the end group order (Fig. 3). Since two different kinetic regions for depolymerizations existed, these were analyzed separately. The results (Fig. 3) indicate that end group orders vary between 0.57 and 1.05, depending on the end group, temperature, and region analyzed. To connect the observed empirical end group orders to the depolymerization mechanisms, we considered three initiation mechanisms and the other expected mechanistic steps: RAFT equilibrium, propagation, depropagation, and termination (Scheme 2).

The first mechanism to consider is an impurity assisted initiation, where an unknown species reacts with the terminal RAFT end group to form an adduct that can decompose to form an active center. If the most dominant initiation mechanism is the initiation by radicals originating from impurities
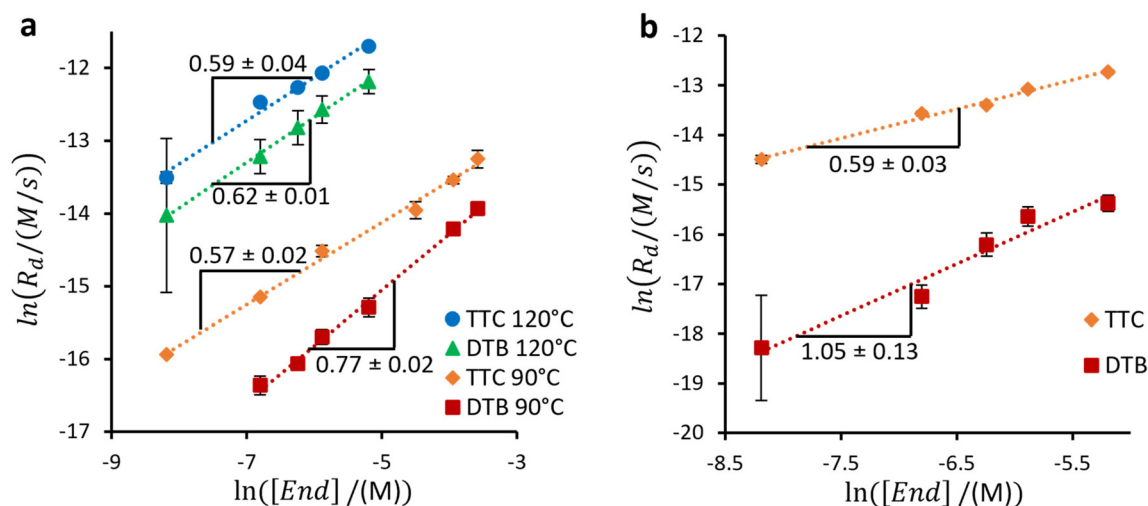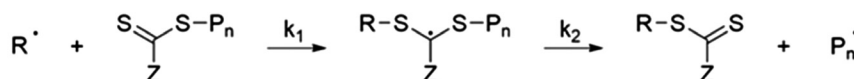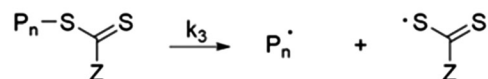

Fig. 3 Polymer end group order plots for PMMA-TTC and PMMA-DTB at 90 and 120 °C using (a) rates expected to include initiation from impurities and the end group (120 °C, 0–15 min; 90 °C, 0–120 min) and (b) rates from regions suspected to have initiation from only the end group (120 °C, 15–60 min). Both end group order plots contain the slopes of each line which indicate the end group order. Errors bars of data points are the standard error of the initial rate. Errors bars of the end group order are the standard error of the linear fit slopes.
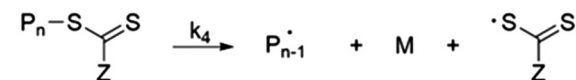
(1) Impurity Assisted Initiation

(2) Initiation by Homolysis

(3) Initiation by Homolysis Accompanied by Monomer Evolution

Scheme 2 Proposed initiation mechanisms involved in RAFT depolymerization.

(Scheme 2, reaction (1)) then the rate of monomer evolution can be expressed as eqn (3) (see SI for derivation):

$$R_d = k_{app1}[\text{End}]^{\frac{1}{2}}[\text{R}^\bullet]^{\frac{1}{2}} \quad (3)$$

where k_{app1} is the apparent rate constant for impurity assisted initiation, [End] is the end group concentration, and $[\text{R}^\bullet]$ is the concentration of radicals generated by impurities. Thus, if only impurities independent of the polymer initiate depolymerization, then the end group order should be 0.5.

The second mechanism is initiation by homolysis, where the C–S bond between the polymer and end group homolyzes to form an active center. If the dominant initiation mechanism is homolysis (Scheme 2, reaction (2)), then the rate of monomer evolution can be expressed as eqn (4) (see SI for derivation):

$$R_d = k_{app2}[\text{End}]^{\frac{1}{2}} \quad (4)$$

where k_{app2} is the apparent rate constant for initiation by homolysis. If the only source of radicals is from homolysis between the RAFT end group and polymer, then the end group order should be 0.5 with respect to the monomer generation for the depolymerization. An order-based analysis cannot differentiate between initiation by C–S homolysis and initiation by solvent derived impurities since they have the same end group order.

The third mechanism is initiation by homolysis accompanied by monomer evolution (Scheme 2, reaction (3)). This mechanism has not been proposed yet for controlled depolymerizations of PMMA, but computational studies on the molecular dynamics of PMMA decomposition suggest it is possible.[43] Stoliarov's simulations suggest that neither random chain scission nor side group scission are dominating initiating steps for PMMA decomposition. Rather, random chain scission accompanied by the evolution of a monomer is the most dominant initiating mechanism. We attempted to observe this homolysis accompanied by monomer evolution using a metadynamic simulation, but under the conditions performed, homolysis was favored. We believe this could be due to the short (two repeat units) length of the PMMA-RAFT analogue used (see SI for more details).

For this reaction, monomers evolve during initiation as well as depropagation of active centers, resulting in eqn (5) (see SI for derivation):

$$R_d = k_{act}[\text{End}]^{\frac{1}{2}} + k_4[\text{End}] \quad (5)$$

where k_{act} is an apparent rate constant associated with monomers evolved from active center concentration, and k_4 is the rate constant for initiation. The first term describes monomers generated by active centers, where k_{act} encompasses k_d and all rate constants that directly affect the active center concentration: initiation by homolysis accompanied by monomer evolution (k_4), RAFT equilibrium (k_{add}, k_{-add}), termination (k_t), and potentially impurity assisted initiation (k_1, k_2). Of the two end groups tested, PMMA-DTB has a RAFT equilibrium that favors the formation of RAFT adducts more than PMMA-TTC,[44] which should reduce the rate of monomer evolution by decreasing the active center concentration. The second term describes monomers generated during initiation. To determine the end group order under various parameters and compare them to experimental data (Fig. 3), the rate at which $\ln(R_d)$ changes with ln can be used to find the order (eqn (6), see SI for derivation):

$$\frac{d \ln(R_d)}{d \ln[\text{End}]} = a = \frac{[\text{End}]^{\frac{1}{2}} + 2m[\text{End}]}{2[\text{End}]^{\frac{1}{2}} + 2m[\text{End}]} \quad (6)$$

where a is the apparent end group order and m is the ratio k_4/k_{act}, which describes a relative propensity of both reactions to generate monomer. As m approaches 0, meaning that monomer evolution is predominantly through depropagating active centers, then a approaches 0.5. If m is large enough that $[\text{End}]^{\frac{1}{2}} \ll m$, then a approaches 1 (Fig. S10). For this model and the end group concentration range of 0.28 to 5.56 mM, different values of m yield apparent end group orders between 0.5 and 1 (Fig. S10). The ratio m would be affected by the RAFT end group, temperature, and solvent since it is composed of rate constants.

Homolysis accompanied by monomer evolution and impurity assisted initiation provides the best explanation for the results observed for PMMA-DTB. At 120 °C, PMMA-DTB has an end group order of 0.62 ± 0.01 for the first 15 minutes. As discussed above (Fig. 2), the initiation of depolymerization is dominated by impurities at first, so the order is near 0.5 due to impurity assisted initiation. Initiation by homolysis, without monomer evolution, is not likely because after the impurities have been consumed at 120 °C, the order of PMMA-DTB is 1.05 ± 0.13, suggesting that monomers are generated during initiation. A fraction of the generated active centers are then converted into RAFT adducts and potentially retarded by the formation of a 3-armed star, similar to how dithiobenzoates retard RAFT polymerizations.[45] Both reactions decrease the rate of depropagation by lowering the active center concentration without irreversible termination, thus, reducing the apparent rate constant k_{act}, increasing the ratio m, and shifting the apparent end group order towards one. At 90 °C, PMMA-DTB has an order of 0.77 ± 0.02, suggesting that initiation by homolysis accompanied by monomer evolution occurs in conjunction with the impurity assisted initiation and/or initiation by homolysis. The lower temperature may prevent irreversible degradation of the end groups that prevents initiation by homolysis at higher temperatures or limit the activation energy available for initiation by homolysis accompanied by monomer evolution or retardation of the depolymerization by 3-arm star formation.

The apparent orders of PMMA-TTC remained between 0.57 and 0.59 under all conditions. PMMA-TTC appears to generate a sufficient concentration of active centers, either through impurities or homolysis, so that depolymerization is not retarded by the TTC end group. DTB is known to retard depolymerizations more than TTC, because the concentration of RAFT adducts at equilibrium for DTB is notably greater.[46] The order of PMMA-TTC is still above 0.5, suggesting that monomers also evolve by the third initiation mechanism and inflating the order of PMMA-TTC to approximately 0.6.

Irreversible destruction of end groups

Since the RAFT end group enables controlled depolymerization, it must be retained throughout the depolymerization to attain maximum conversion. For example, PMMA-DTB is known in literature to undergo end group loss by Chugaev-like elimination at 150 °C.[47] The degradation of PMMA-DTB end groups in 1,4-dioxane has also been observed during depolymerization and was attributed to Chugaev-like elimination, disproportionation, and/or hydrolysis.[12] These reactions, excluding disproportionation, are also expected to be dependent on the lability of the RAFT end group in a particular solvent. We explored the irreversible destruction of PMMA-TTC and PMMA-DTB in toluene to understand how it differs from solvents with higher depolymerization rates like 1,4-dioxane.

During depolymerizations, the end group peaks in NMR spectra decreased in intensity relative to the MMA methyl protons located on repeat units and monomers, indicating irreversible degradation (Fig. 4a and b). The end group concentration was monitored over time and revealed that both end groups degrade at similar rates (Fig. 4c). The degradation of both end groups followed first order kinetics, resulting in a half-life of 21 h for both PMMA-DTB and PMMA-TTC (Fig. 4d). This result is interesting because the PMMA-DTB depolymerized slower due to lower apparent active center concentrations, which we hypothesized was due to irreversible termination of the end groups after initiation. If end group degradation is assumed as a side product of initiating depolymerizations, similar degradation rates could be expected to lead to similar depolymerization rates provided the RAFT end groups have similar RAFT equilibria. This observed discrepancy suggests that another end group decomposition route exists that allows DTB end groups to decay as fast as TTC without resulting in similar depolymerization rates in toluene.

Chong et al. found that the depolymerization PMMA-DTB in the melt exhibits an initial mass loss between 150 and 220 °C that was attributed to the loss of end group.[36] They hypothesized that PMMA-DTB was more susceptible to Chugaev elimination (Fig. 4f), yielding unsaturated end groups. PMMA-TTC was more susceptible to homolysis, allowing active centers to generate and yield monomer. We believe we witnessed the same phenomena in toluene at 120 °C. Thus, the similar end group decomposition rates but different depolymerization rates are likely due to the relative propensity for PMMA-TTC and PMMA-DTB to initiate as opposed to a Chugaev elimination in solution.

To confirm the different propensities towards homolysis and elimination, we monitored the unsaturated polymer end group concentration ([Unsat]) that could be due to the elimination of the RAFT end group (Fig. 4e) or termination by disproportionation. Clear signals from the unsaturated end group were visible in HNMR spectroscopy (Fig. S11), confirming the formation of these end groups. Within 96 hours, PMMA-TTC generates 1.8 mM of unsaturated end groups while PMMA-DTB generates 4.3 mM. Assuming all RAFT end groups undergo elimination, the maximum [Unsat] is the initial RAFT end group concentration (5.56 mM). If the [Unsat] was only generated by disproportionation of active centers, then the maximum [Unsat] would be half the initial RAFT end group concentration (2.78 mM). PMMA-DTB had a final unsaturated end group concentration of 4.34 mM, greater than that from solely disproportionation, supporting the existence of Chugaev elimination. However, the products of Chugaev elimination, dithiocarbonic acids with the appropriate Z group, were not visible in the ^{1}H NMR spectra. After the PMMA-DTB end group completely degraded, new aromatic peaks appeared that could originate from the degradation of the end group, degradation of the dithiocarbonic acid, or side reactions with residual toluene (Fig. S12). For PMMA-TTC, end group degradation was accompanied by the evolution of 1-dodecanethiol (Fig. S13). This product is likely a result of the PMMA-TTC end group thermally degrading to form carbon disulfide and 1-dodecanethiol. Our metadynamic simulations have found that while the Chugaev elimination is a potential pathway for PMMA-RAFT polymers (see SI for details), the activation
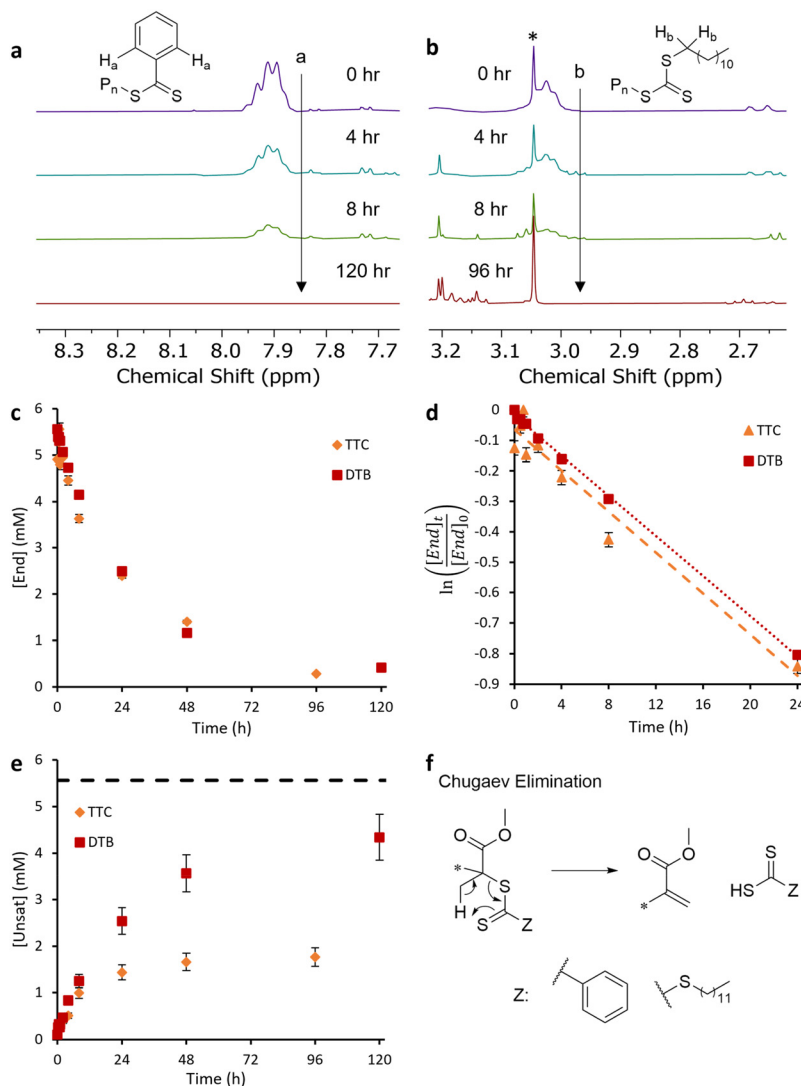
Fig. 4 ^{1}H NMR spectra of (a) PMMA-DTB and (b) PMMA-TTC end group protons over time. The end group concentration was 5.56 mM in toluene-d8, with the temperature held at 120 °C. PMMA-TTC had a methanol peak interfering with the alpha methylene protons of TTC that remained after 96 h (marked by an asterisk). (c) End group concentration ([End]) as a function of time for PMMA-TTC and PMMA-DTB depolymerizations (120 °C and [End]$_0$ = 5.56 mM). (d) Linearized degradation kinetics assuming a first-order kinetics model. (e) Concentration of unsaturated ends ([Unsat]) of PMMA-TTC and PMMA-DTB depolymerizations over time (120 °C and [End]$_0$ = 5.56 mM). The dashed black line at 5.56 mM indicates the maximum possible [Unsat] assuming all polymers undergo elimination. (f) Mechanism of the Chugaev elimination. Error bars are one standard error with n = 2 replications.

energy is significantly higher than depolymerization, which further suggests that elimination does not occur through a Chugaev elimination. Likely an elimination pathway exists for PMMA-DTB that is neither a Chugaev elimination nor disproportionation that is tied to the degradation of DTB end group. The greater tendency of PMMA-DTB to irreversibly terminate through elimination in toluene suggests that the propensity for an end group to eliminate is another factor to optimize for PMMA-RAFT depolymerizations under different conditions. Successful reduction of the elimination rate by synthesizing novel RAFT agents will result in depolymerizations with fewer dead polymers generated and higher monomer yields.

Computational analysis of mechanism

The empirical data above enables the opportunity to explore further the mechanisms described. We performed metadynamics simulations to model the initiation and elimination mechanisms, compare experiments to theory, and predict the reactivity of untested RAFT end groups (see SI for more details). Throughout the initiation simulation, the C–S bond broke in a homolytic manner leaving behind radicals on carbon and sulfur (Fig. 5a and b). Based on preliminary DFT simulations, achieving a simultaneous C–C homolytic cleavage was challenging (Scheme 2, reaction (3)), because of the high thermal stability of the C–C bond. The absence
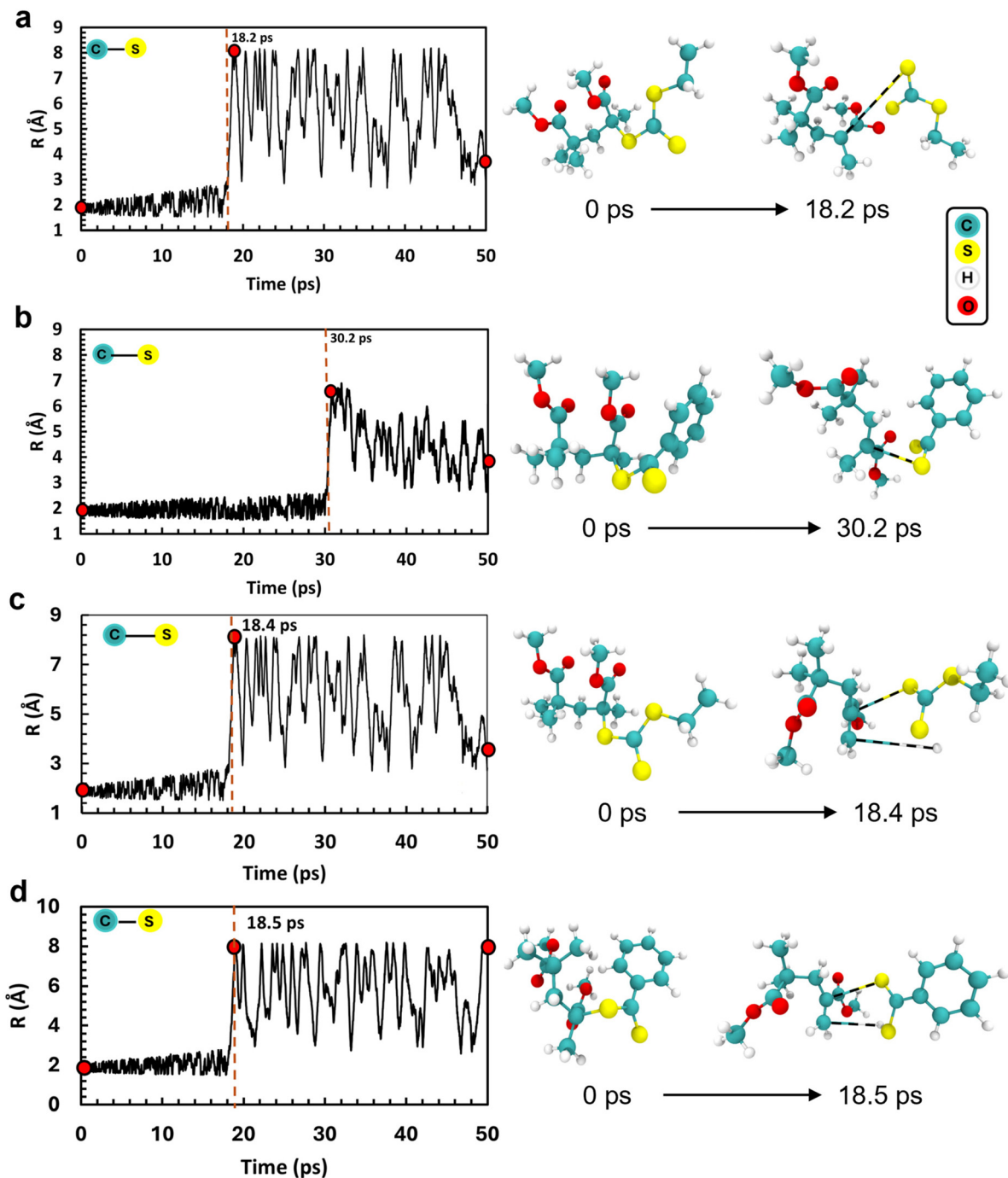
Fig. 5 Variation of C–S bond distances throughout initiation for (a) PMMA-TTC and (b) PMMA-DTB, and over time. The C–S bond is cleaved after 18.2 ps and 30.2 ps for PMMA-TTC and PMMA-DTB, respectively. Variation of C–S bond distances throughout elimination for (c) PMMA-TTC and (d) PMMA-DTB, and over time. The C–S bond is cleaved after 18.4 ps and 18.5 ps for PMMA-TTC and PMMA-DTB, respectively. Snapshots are provided of PMMA-TTC and PMMA-DTB before and after bond cleavage.

of the simultaneous C–C and C–S bond stretching associated with simultaneous initiation and monomer evolution may be attributed to the molecule consisting of only two monomers. Simulation of larger polymers would be more representative of the conformational and entropic effects on the depolymerization thermodynamics potentially

demonstrating simultaneous initiation and monomer release.

Throughout the elimination simulation, the C–S and C–H bonds broke concertedly. For simulations of TTC, DTB, 1-pyrrolecarbodithioate (DTP), and *N*-pyridine carbonodithiaote (PCDT) (Fig. 5c, d, S17, and S18, respectively) the elimination

occurs much like the Chugaev elimination described in Fig. 4f, but at high enough activation energies that suggest this mechanism is not likely to occur which is consistent with previous literature.[48,49] These computational results support the inherent challenge with the experimentally observed irreversible termination through elimination that competes with depolymerization, while only relying on thermal initiation through the end group homolysis. Interestingly, the elimination of DTO resulted in the direct formation of carbon disulfide and ethanol (Fig. S16) demonstrating that expanding the scope of RAFT end groups for controlled depolymerizations may result in additional degradation mechanisms to investigate.

The time required to achieve bond cleavage in the metadynamics simulations represents the potential well that must be filled for the bond cleavage to be spontaneous. For initiation, the cleavage of the C–S bond takes place after 18.2 ps and 30.2 ps for TTC and DTB, respectively. The greater time required for bond cleavage of C–S in DTB relative to TTC demonstrates the lower lability of DTB towards initiation and subsequent depolymerization, as observed in the empirical analysis. For depropagation, the cleavage of the C–C bond between MMA repeat units takes place after 6.1 ps (Fig. S19). The shorter time required for C–C bond cleavage compared to C–S bond cleavage suggests that once initiation occurs, depropagation is rapid. DTO, DTP, and PCDT achieved bond cleavage in 43.1 ps, 42.3 ps, 40.8 ps (Fig. S20–S22), suggesting that these RAFT end groups would not be ideal candidates for depolymerizations due to sluggish initiation relative to TTC. Interestingly, the gas phase computational results are consistent with our results in toluene, but different from those reported in 1,4-dioxane, indicating that 1,4-dioxane plays a more significant role in affecting the rate of depolymerization. Additionally, no observed correlation existed between the lability of the RAFT end group towards homolysis and the radical stabilization energy of their respective RAFT adducts.[44] Instead, the lability appears to correlate with the radical stability of the RAFT group fragment after homolysis (see SI for more details). As for elimination, the cleavage of the C–S bond in TTC and DTB takes place after 18.4 ps and 18.5 ps respectively, exhibiting similar barriers to elimination. Furthermore, the time required for bond cleavage *via* initiation was 63% greater than that of elimination for DTB, which supports the empirical findings of DTB having a greater propensity towards elimination, suggesting that toluene does not play a significant role in the reactivity of the RAFT end groups during these polymerizations.

External radical addition

To hasten RAFT depolymerizations, scientists have used light,[34] excess heat,[17,37] and photocatalysts[50–52] to promote initiation. More recently, the Anastasaki group employed azo and peroxide thermal initiators to promote the depolymerization of polymethacrylate and poly(methacrylamides).[49,53] They found that adding azo initiators in lower monomer yield solvents for depolymerization, such as 1,2,4-trichlorobenzene,

can increase the depolymerization rate and final conversion for polymethacrylates. This increase in conversion made these solvents a potential replacement for 1,4-dioxane, as it eliminates the need for the radicals derived from dioxane and its impurities. No literature compares the differences between DTB and TTC end groups in depolymerizing polymethacrylates in a lower monomer yield solvent for depolymerization with thermal initiators. To investigate the effects of hard and soft radicals, we used di-*tert*-butyl peroxide (DTBP) and azobisisobutyronitrile (AIBN) initiators, respectively. We anticipated that soft radicals formed by AIBN would initiate PMMA-RAFT directly to allow depolymerization. On the other hand, we expected hard radicals from DTBP to not initiate PMMA-RAFT directly due to the poor reactivity between oxygen centered radicals and carbon–sulfur pi bonds.[54] To this end, we analyzed the order and monomer yields of depolymerizations with DTBP at 120 °C and AIBN at 90 °C (Fig. 6). Moreover, DTBP at 120 °C and AIBN at 90 °C were expected to have different half-lives, 20 h and 26 min, respectively, allowing us to explore how the rate of initial radical generation affects the rate of depolymerization.

Depolymerizations with AIBN were monitored over extended periods to see the effect of AIBN on the yielded monomer concentration (Fig. 6a and b). Increasing the concentration of AIBN yielded higher monomer concentrations for depolymerizations with PMMA-TTC, yielding the highest monomer concentration with 0.3 [AIBN]:[End] at 6 h. For the depolymerization of PMMA-DTB the yield always increased with increasing concentration of AIBN. The depolymerizations were continued for 4–5 days (Fig. S25) at 90 °C to see the long-term effects of depolymerizing with AIBN. The half-life of AIBN in benzene at 90 °C is expected to be 26 minutes, so monitoring a depolymerization for this long shows the ability of the polymers to self-initiate after being assisted by an exogenous radical species.[55] For PMMA-TTC, a 0.1 [AIBN]:[End] yielded the greatest monomer concentration, while values higher than 0.1 resulted in monomer concentrations below that of no added initiator. For PMMA-DTB without AIBN, the long-term depolymerization yielded the lowest monomer concentration as increasing [AIBN] resulted in higher monomer concentration.

When using AIBN as an initiator for the depolymerization of PMMA with DTB and TTC end groups at 90 °C, the rate dependence and order of the AIBN concentration varies (Fig. 6c). At AIBN concentrations below 1.11 mM, the initial depolymerization rate increased with increasing concentrations of AIBN. Above this value, adding more AIBN no longer increased the initial rate of monomer evolution likely because the radicals generated by AIBN can promote both initiation and termination. At low concentrations, AIBN fragments into radicals that can react with RAFT end groups to generate active centers. The concentration of active centers is then held at a low concentration due to the formation of RAFT adducts in a controlled depolymerization, leading to minimal termination. When an excessive amount of AIBN is introduced, the concentration of active centers, AIBN fragments, and RAFT

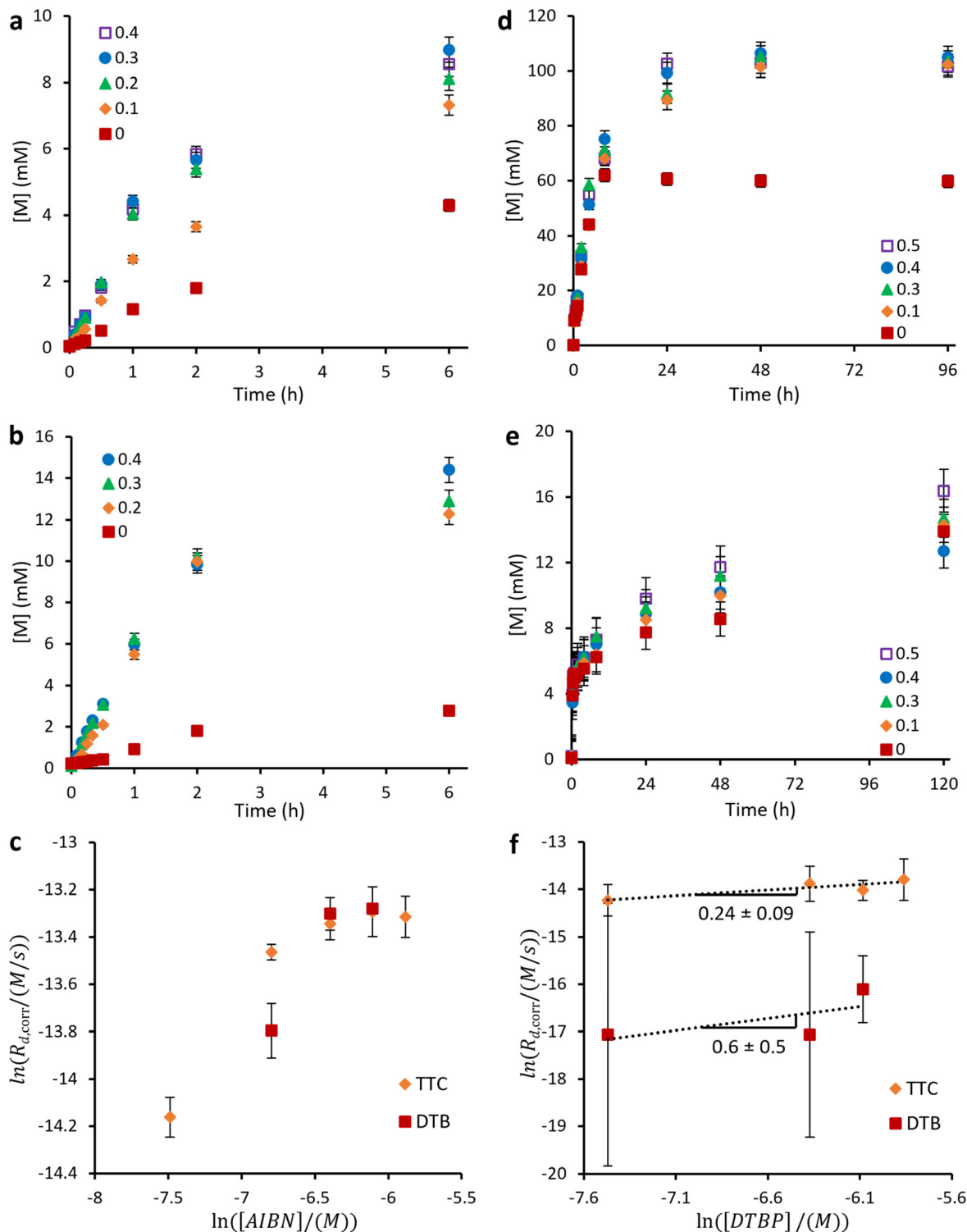

Fig. 6 Depolymerization curves of (a) PMMA-TTC and (b) PMMA-DTB at 90 °C with varying [AIBN] : [End] as indicated by legends. Order analysis of added (c) AIBN at 90 °C. Depolymerization curves of (d) PMMA-TTC and (e) PMMA-DTB at 120 °C with varying [DTBP] : [End] as indicated by legends. Order analysis of added (f) DTBP at 120 °C. All reactions were performed with an end group concentration of 5.56 mM, or 200 mM repeat unit concentration, in toluene-d8. Error bars of graphs (a), (b), (d) and (e) are one standard error with n = 2 replications. Error bars of graphs (c) and (f) are from the standard error of the initial rate.

adducts are high and termination becomes more prevalent.[56] For higher AIBN concentrations the excess AIBN initiates and terminates active centers, resulting in similar initial depolymerization rates.

The differences in depolymerization rates and final conversions for varying end groups and concentrations of AIBN have straightforward explanations. As the order suggests, low concentrations of AIBN predominantly initiate RAFT end groups to generate monomers faster, but an excess of AIBN saturates the reaction with radicals and promotes termination. Consequently, initially more monomers evolved due to the high active center concentration. Later in the reaction, lower AIBN concentrations yield more monomers because fewer polymers have been irreversibly terminated at the beginning of the depolymerization. Interestingly, PMMA-DTB exhibited faster depolymerization rates than PMMA-TTC at equivalent concentrations of AIBN. This finding suggests that the DTB end group is more readily initiated from exogenous carbon-centered radical species, which is consistent with depolymerizations of PMMA-DTB being faster than PMMA-TTC in 1,4-dioxane.[12] Solvent derived carbon-centered radicals are known to initiate depolymerization in 1,4-dioxane,[14] and this initiation mechanism likely enhances the depolymerization rate of PMMA-DTB more favorably. Apparently, lower monomer yield depolymerization solvents such as toluene lack a significant concentration of solvent derived carbon-centered radicals, resulting in PMMA-TTC self-initiating more readily and achieving higher yields than PMMA-DTB.

Depolymerizations with DTBP at 120 °C behaved differently than AIBN-based depolymerizations. For PMMA-TTC samples, the first two hours yielded similar monomer concentrations regardless of the [DTBP] (Fig. 6d and e). After depolymerizing for more than 2 days, PMMA-TTC samples that contained peroxides yielded a monomer concentration ~40 mM greater than the sample without peroxides. The degree to which PMMA-TTC depolymerized was observable in the SEC (Fig. S26) with a shift in the curves towards higher retention times, suggesting that the depolymerization is controlled in the presence of DTBP. Adding peroxides to PMMA-DTB did not significantly affect initial rates and yielded similar monomer concentrations throughout the depolymerization. SEC showed a slight shift in molecular weight with minimal differences between samples with and without peroxides (Fig. S27), indicating limited depolymerization.

Using DTBP as a depolymerization initiator, we found that the orders for [DTBP] for the overall reaction were 0.24 ± 0.09 and 0.6 ± 0.5 for PMMA-TTC and PMMA-DTB, respectively (Fig. 6f). These orders are essentially zero with significant error, suggesting that peroxides have little effect on the initial depolymerization rates. Since the half-life of DTBP is 20 h, the concentration of radicals produced at any time would be significantly lower than AIBN at the same time point and thus, may explain the lack of effect on the initial rate for DTBP as compared to AIBN. Additionally, DTBP could take part in hydrogen abstraction side reactions that were not productive for initiation, limiting its effect. The order analysis and the

difference in final monomer yields suggest that DTBP increased the monomer yield of PMMA-TTC by reacting with monomers that in turn reacted with the RAFT end groups to increase monomer yields. The ultimate conversion of PMMA-DTB does not increase with DTBP addition because the monomer concentration was too low for peroxides to react with monomer at a significant rate. This differs from the results of polymethacrylamides in 10% DMSO/90% 1,4-dioxane solvents[49] likely because DTBP can react with dioxane, which can then initiate PMMA-DTB. On the other hand, depolymerization of PMMA-TTC achieved sufficient monomer concentration to react with peroxides, creating carbon-centered radicals to promote the reaction. In doing so, all PMMA-TTC depolymerizations with DTBP reached the equilibrium monomer concentration, as confirmed by our polymerizations at 120 °C (Table S1).

For the depolymerizations with AIBN and DTBP, the use of peroxides at 120 °C with PMMA-TTC is promising for chemical recycling due to faster rates and higher monomer yields at higher repeat unit concentrations than reported in literature for this end group. AIBN had a positive effect on initial depolymerization rates, and with optimization, improved the monomer concentration yield. The increase in depolymerization rates was likely because AIBN produces carbon centered radicals that can react with the RAFT end groups directly to form active centers. For DTBP, the initial rates were not affected to such an extent, but the monomer concentration was greater due to the reactivity of DTBP with monomers to produce carbon centered radicals that react with RAFT end groups. The data from AIBN and DTBP aided depolymerizations suggest that a high temperature thermal initiator that directly generates carbon-centered radicals would be the best initiator for chemical recycling. However, these types of commercially available thermal initiators are not common and thus, we were unable to test this hypothesis at this time.

Conclusions

PMMA-RAFT thermal depolymerizations in a typically lower monomer yield depolymerization solvent, toluene, are still assisted by solvent-derived impurities like those observed in 1,4-dioxane. The stability of different RAFT agents leads to the observed differences in depolymerization rate and extent of monomer evolution due to different initiation mechanisms. The order-based analysis also revealed differences between the dominant mechanisms of PMMA-TTC and PMMA-DTB depolymerization depending on temperatures and depolymerization time. Most of the monomers for the PMMA-TTC depolymerization evolved from active centers due to either impurity assisted initiation or C–S homolysis. However, PMMA-DTB had orders that indicated that monomers were generated by the initiation of PMMA-RAFT once the impurities were consumed. Additionally, PMMA-DTB is more susceptible to elimination than PMMA-TTC under these conditions, which affects the ultimate monomer yield and depolymerization rates. This

difference suggests that the RAFT agent and solvent pair could be optimized to lower the rate of elimination for more effective depolymerizations. Furthermore, adding exogenous radical initiators can enhance the rate of depolymerization and yield of monomers when paired with PMMA-TTC through the generation of additional active centers. These findings show that controlled depolymerizations of PMMA *via* RAFT have multiple factors to be optimized.

Author contributions

Empirical: All synthetic and analytical methods were performed by Don Bones under the supervision of Dr William Gramlich. The write-up of the empirical results was done by Don Bones under the supervision of Dr William Gramlich.

Computational: An initial quantum mechanics-based survey of potential RAFT agents was carried out by Emily Nelson and Bryanna Fofie (both undergraduates) under the supervision of Dr Erik P. Hoy to provide insights into the expected activation energies of RAFT agents and provide insights into potential decomposition mechanisms. This informed the design of the final mechanism and dynamics studies that were designed and carried out by Adarsh Kumar (graduate student) under the supervision of Dr Erik P. Hoy. The write-up of the computational results was done by Mr Kumar under the supervision of Dr Hoy.

Conflicts of interest

There are no conflicts to declare.

Data availability

The data supporting this article have been included as part of the supplementary information (SI). Supplementary information is available, which includes derivations of kinetics equations, computational analysis descriptions, additional NMR spectra, and additional kinetics results. See DOI: https://doi.org/10.1039/d5py00576k.

Acknowledgements

References

1 S. M. Al-Salem, P. Lettieri and J. Baeyens, *Waste Manage.*, 2009, **29**, 2625–2643.

2 J. Jiang, K. Shi, X. Zhang, K. Yu, H. Zhang, J. He, Y. Ju and J. Liu, *J. Environ. Chem. Eng.*, 2022, **10**, 106867.

3 G. Lopez, M. Artetxe, M. Amutio, G. Elordi, R. Aguado, M. Olazar and J. Bilbao, *Chem. Eng. Process. Process Intensif.*, 2010, **49**, 1089–1094.

4 G. R. Jones, H. S. Wang, K. Parkatzidis, R. Whitfield, N. P. Truong and A. Anastasaki, *J. Am. Chem. Soc.*, 2023, **145**, 9898–9915.

5 R. W. Hughes, M. E. Lott, I. S. Zastrow, J. B. Young, T. Maity and B. S. Sumerlin, *J. Am. Chem. Soc.*, 2024, **146**, 6217–6224.

6 M. R. Martinez, D. Schild, F. De Luca Bossa and K. Matyjaszewski, *Macromolecules*, 2022, **55**, 10590–10599.

7 S. Huang, X. Su, Y. Wu, X.-G. Xiong and Y. Liu, *Chem. Sci.*, 2022, **13**, 11352–11359.

8 D. J. Keddie, G. Moad, E. Rizzardo and S. H. Thang, *Macromolecules*, 2012, **45**, 5321–5342.

9 M. J. Flanders and W. M. Gramlich, *Polym. Chem.*, 2018, **9**, 2328–2335.

10 H. S. Wang, N. P. Truong, Z. Pei, M. L. Coote and A. Anastasaki, *J. Am. Chem. Soc.*, 2022, **144**, 4678–4684.

11 K. S. C. Jäger, G. D. Ammini, P.-J. Voorter, P. Subramanian, A. Kumar, A. Anastasaki and T. Junkers, *J. Am. Chem. Soc.*, 2024, **147**, 594–602.

12 H. S. Wang, N. P. Truong, G. R. Jones and A. Anastasaki, *ACS Macro Lett.*, 2022, **11**, 1212–1216.

13 N. D. A. Watuthanthrige, A. Moskalenko, A. A. Kroeger, M. L. Coote, N. P. Truong and A. Anastasaki, *Chem. Sci.*, 2025, **16**, 3516–3522.

14 F. Häfliger, N. P. Truong, H. S. Wang and A. Anastasaki, *ACS Macro Lett.*, 2023, **12**, 1207–1212.

15 G. Moad, Y. K. Chong, A. Postma, E. Rizzardo and S. H. Thang, *Polymer*, 2005, **46**, 8458–8468.

16 J. Chiefari, Y. K. (Bill) Chong, F. Ercole, J. Krstina, J. Jeffery, T. P. T. Le, R. T. A. Mayadunne, G. F. Meijs, C. L. Moad, G. Moad, E. Rizzardo and S. H. Thang, *Macromolecules*, 1998, **31**, 5559–5562.

17 R. Whitfield, G. R. Jones, N. P. Truong, L. E. Manring and A. Anastasaki, *Angew. Chem., Int. Ed.*, 2023, **62**, e202309116.

18 Y. Zhao and D. G. Truhlar, *Theor. Chem. Acc.*, 2008, **120**, 215–241.

19 F. Weigend and R. Ahlrichs, *Phys. Chem. Chem. Phys.*, 2005, **7**, 3297–3305.

20 M. J. Frisch, G. W. Trucks, H. B. Schlegel, G. E. Scuseria, M. A. Robb, J. R. Cheeseman, G. Scalmani, V. Barone, G. A. Petersson, H. Nakatsuji, X. Li, M. Caricato, A. V. Marenich, J. Bloino, B. G. Janesko, R. Gomperts, B. Mennucci, H. P. Hratchian, J. V. Ortiz, A. F. Izmaylov, J. L. Sonnenberg, D. Williams-Young, F. Ding, F. Lipparini, F. Egidi, J. Goings, B. Peng, A. Petrone, T. Henderson, D. Ranasinghe, V. G. Zakrzewski, J. Gao, N. Rega, G. Zheng, W. Liang, M. Hada, M. Ehara, K. Toyota, R. Fukuda,

J. Hasegawa, M. Ishida, T. Nakajima, Y. Honda, O. Kitao, H. Nakai, T. Vreven, K. Throssell, J. A. Montgomery Jr., J. E. Peralta, F. Ogliaro, M. J. Bearpark, J. J. Heyd, E. N. Brothers, K. N. Kudin, V. N. Staroverov, T. A. Keith, R. Kobayashi, J. Normand, K. Raghavachari, A. P. Rendell, J. C. Burant, S. S. Iyengar, J. Tomasi, M. Cossi, J. M. Millam, M. Klene, C. Adamo, R. Cammi, J. W. Ochterski, R. L. Martin, K. Morokuma, O. Farkas, J. B. Foresman and D. J. Fox, *Gaussian 16, Revision C.01*.

21 J. Zhang and M. Dolg, *Phys. Chem. Chem. Phys.*, 2016, **18**, 3003–3010.

22 J. Zhang and M. Dolg, *Phys. Chem. Chem. Phys.*, 2015, **17**, 24173–24181.

23 T. D. Kühne, M. Iannuzzi, M. Del Ben, V. V. Rybkin, P. Seewald, F. Stein, T. Laino, R. Z. Khaliullin, O. Schütt, F. Schiffmann, D. Golze, J. Wilhelm, S. Chulkov, M. H. Bani-Hashemian, V. Weber, U. Borštnik, M. Taillefumier, A. S. Jakobovits, A. Lazzaro, H. Pabst, T. Müller, R. Schade, M. Guidon, S. Andermatt, N. Holmberg, G. K. Schenter, A. Hehn, A. Bussy, F. Belleflamme, G. Tabacchi, A. Glöß, M. Lass, I. Bethune, C. J. Mundy, C. Plessl, M. Watkins, J. VandeVondele, M. Krack and J. Hutter, *J. Chem. Phys.*, 2020, **152**, 194103.

24 J. VandeVondele, M. Krack, F. Mohamed, M. Parrinello, T. Chassaing and J. Hutter, *Comput. Phys. Commun.*, 2005, **167**, 103–128.

25 S. Goedecker, M. Teter and J. Hutter, *Phys. Rev. B: Condens. Matter Mater. Phys.*, 1996, **54**, 1703–1710.

26 C. Hartwigsen, S. Goedecker and J. Hutter, *Phys. Rev. B: Condens. Matter Mater. Phys.*, 1998, **58**, 3641–3662.

27 J. VandeVondele and J. Hutter, *J. Chem. Phys.*, 2007, **127**, 114105.

28 J. P. Perdew, K. Burke and M. Ernzerhof, *Phys. Rev. Lett.*, 1996, **77**, 3865–3868.

29 S. Grimme, J. Antony, S. Ehrlich and H. Krieg, *J. Chem. Phys.*, 2010, **132**, 154104.

30 G. Bussi, D. Donadio and M. Parrinello, *J. Chem. Phys.*, 2007, **126**, 014101.

31 G. Lippert and J. Hutter, *Mol. Phys.*, 1997, **92**, 477–488.

32 B. Ensing, A. Laio, M. Parrinello and M. L. Klein, *J. Phys. Chem. B*, 2005, **109**, 6676–6687.

33 I. Kaliman, A. Nemukhin and S. Varfolomeev, *J. Chem. Theory Comput.*, 2010, **6**, 184–189.

34 J. B. Young, J. I. Bowman, C. B. Eades, A. J. Wong and B. S. Sumerlin, *ACS Macro Lett.*, 2022, **11**, 1390–1395.

35 M. Z. Bekanova, N. K. Neumolotov, A. D. Jablanović, A. V. Plutalova, E. V. Chernikova and Y. V. Kudryavtsev, *Polym. Degrad. Stab.*, 2019, **164**, 18–27.

36 B. Chong, G. Moad, E. Rizzardo, M. Skidmore and S. H. Thang, *Aust. J. Chem.*, 2006, **59**, 755.

37 J. B. Young, R. W. Hughes, A. M. Tamura, L. S. Bailey, K. A. Stewart and B. S. Sumerlin, *Chem*, 2023, **9**, 2669–2682.

38 C. Reichardt, T. Welton, In *Solvents and Solvent Effects in Organic Chemistry*, John Wiley & Sons, Ltd, 2010, pp. 165–357.

39 Liquids – Dielectric Constants, https://www.engineeringtoolbox.com/liquid-dielectric-constants-d_1263.html, (accessed September 5, 2024).

40 Y. Gu, J. Zhao, Q. Liu, X. Pan, W. Zhang, Z. Zhang and X. Zhu, *Polym. Chem.*, 2015, **6**, 359–363.

41 P. Maximiano, P. V. Mendonça, J. R. C. Costa, N. L. Haworth, A. C. Serra, T. Guliashvili, M. L. Coote and J. F. J. Coelho, *Macromolecules*, 2016, **49**, 1597–1604.

42 D. C. Mielczarek, M. Matrat, A. B. Amara, Y. Bouyou, P. Wund and L. Starck, *Energy Fuels*, 2017, **31**, 12893–12913.

43 S. I. Stoliarov, P. R. Westmoreland, M. R. Nyden and G. P. Forney, *Polymer*, 2003, **44**, 883–894.

44 E. H. Krenske, E. I. Izgorodina and M. L. Coote, in *Controlled/Living Radical Polymerization*, American Chemical Society, 2006, vol. 944, pp. 406–420.

45 G. Moad, J. Chiefari, Y. K. (Bill) Chong, J. Krstina, R. T. Mayadunne, A. Postma, E. Rizzardo and S. H. Thang, *Polym. Int.*, 2000, **49**, 993–1001.

46 W. Meiser and M. Buback, *Macromol. Rapid Commun.*, 2011, **32**, 1490–1494.

47 B. Chong, G. Moad, E. Rizzardo, M. Skidmore and S. H. Thang, *Aust. J. Chem.*, 2006, **59**, 755.

48 F. Felician, M.-N. Antonopoulou, N. P. Truong, A. A. Kroeger, M. L. Coote, G. R. Jones and A. Anastasaki, *Polym. Chem.*, 2025, **16**, 1822–1828.

49 V. Lohmann, G. R. Jones, A. A. Kroeger, N. P. Truong, M. L. Coote and A. Anastasaki, *Angew. Chem., Int. Ed.*, 2025, e202425575.

50 V. Bellotti, K. Parkatzidis, H. S. Wang, N. D. A. Watuthanthrige, M. Orfano, A. Monguzzi, N. P. Truong, R. Simonutti and A. Anastasaki, *Polym. Chem.*, 2023, **14**, 253–258.

51 V. Bellotti, H. S. Wang, N. P. Truong, R. Simonutti and A. Anastasaki, *Angew. Chem., Int. Ed.*, 2023, **62**, e202313232.

52 G. Ng, S. W. Prescott, A. Postma, G. Moad, C. J. Hawker, A. Anastasaki and C. Boyer, *J. Polym. Sci.*, 2024, **62**(17), 3920–3928, DOI: 10.1002/pol.20240255.

53 D. Mantzara, R. Whitfield, H. S. Wang, N. P. Truong and A. Anastasaki, *ACS Macro Lett.*, 2025, 235–240.

54 I. Fleming, in *Molecular Orbitals and Organic Chemical Reactions*, John Wiley & Sons, Ltd, 2010, pp. 369–400.

55 J. Bandrup, E. Immergut and E. Grulke, *Polymer Handbook*, John Wiley & Sons, 4th edn, 2005.

56 G. Moad, Y. K. Chong, R. Mulder, E. Rizzardo and S. H. Thang, in *Controlled/Living Radical Polymerization: Progress in RAFT, DT, NMP & OMRP*, ed. K. Matyjaszewski, American Chemical Society, Washington, DC, 2009, vol. 1024, pp. 3–18.